

Photodissociation dynamics of $\text{Li}(\text{NH}_3)_4$: a velocity map imaging study.

W. Scott Hopkins¹, Alex P. Woodham¹, Nicola M. Tonge², Andrew M. Ellis^{2} and Stuart R. Mackenzie^{1*}*

1. Department of Chemistry, University of Oxford, South Parks Road, Oxford, OX1 3QZ, UK

2. Department of Chemistry, University of Leicester, University Road, Leicester, LE1 7RH, UK

Andrew Ellis: andrew.ellis@le.ac.uk

Stuart Mackenzie: stuart.mackenzie@chem.ox.ac.uk

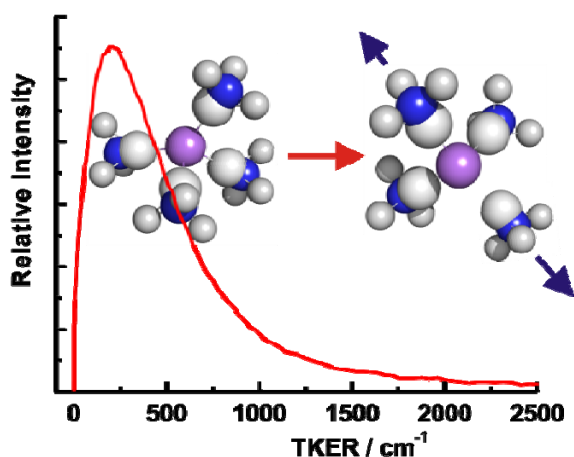
RECEIVED DATE

Andrew Ellis Contact Information: Tel +44(0) 116 252 2138; Fax +44(0) 116 252 3789

Stuart Mackenzie Contact Information: Tel +44(0) 186 527 5156; Fax +44(0) 186 527 5410

Abstract

The photodissociation dynamics of alkali-ammonia clusters in the gas phase have been explored using a combination of photofragmentation spectroscopy and velocity map imaging. Electronic excitation of $\text{Li}(\text{NH}_3)_4$ to the \tilde{A}^2T_2 state leads to the production of relatively slow photofragments with a high degree of internal excitation, consistent with internal conversion to the ground electronic state of $\text{Li}(\text{NH}_3)_4$ followed by slow, statistical decay. At low excitation energies the dominant decay channel yields $\text{Li}(\text{NH}_3)_3 + \text{NH}_3$, but at higher energies $\text{Li}(\text{NH}_3)_2$ is the dominant lithium-containing photoproduct. Evidence for a barrier in the exit channel is provided by the distinct maximum in the total kinetic energy release (TKER) distribution observed at low kinetic energy. Modeling of the TKER distribution for the $\text{Li}(\text{NH}_3)_4 \rightarrow \text{Li}(\text{NH}_3)_3 + \text{NH}_3$ process suggests an upper limit of $3750 \pm 150 \text{ cm}^{-1}$ for the Li-N bond dissociation energy and a barrier height of approximately $150 \pm 50 \text{ cm}^{-1}$.



Keywords: Alkali-ammonia, lithium, photodissociation, statistical decay, density of states, exit channel barrier

The incorporation of electrons in solvents has been of interest for many decades and has practical significance in that these electrons can induce chemical reactions upon encountering susceptible molecules. One important example is DNA, which can be damaged by low energy electrons generated by the passage of ionizing radiation through biological samples.¹ One of the most familiar sources of solvated electrons is produced by dissolving an alkali metal in liquid ammonia – a process first observed in the laboratory more than two centuries ago by Humphry Davy.² Under very dilute conditions the solutions are blue and this color has long been attributed to the absorption of light by solvated electrons. There is, however, a surprising lack of detailed understanding of these solutions at the molecular level. This extends from ongoing debates about the optical absorption profile³ to the actual chemical species present in the solutions at various concentrations. With regard to the latter, Zurek and co-workers recently reported a comprehensive series of density functional theory calculations of potentially important species in lithium/ammonia solutions.⁴ In addition to solvated electrons, the species $\text{Li}(\text{NH}_3)_4$ is a recurring theme in these calculations. However, given possible contributions from both larger and smaller complexes, as well as charged variants, experimental confirmation of the presence and role of $\text{Li}(\text{NH}_3)_4$ in lithium/ammonia solutions remains speculative and is inferred rather than proven.

In one of our laboratories we have recently undertaken a series of spectroscopic studies seeking to identify and characterize alkali metal atom/ammonia complexes *in the gas phase*.⁵⁻⁸ One of the aims of this programme of work is to provide information on the isolated complexes free of i) interference from other individual species and ii) the perturbation provided by any bulk solvent. Intriguingly, the observed absorption profile of $\text{Li}(\text{NH}_3)_4$ has much in common with the spectral profile of the electron in bulk liquid ammonia.⁸ It has been suggested that the similarity between the spectrum of $\text{Li}(\text{NH}_3)_4$ and that of an electron in bulk liquid ammonia is not accidental, but rather derives from the already diffuse nature of the unpaired electron in both the ground and excited electronic states of $\text{Li}(\text{NH}_3)_4$.⁴

The electronic spectrum of $\text{Li}(\text{NH}_3)_4$ was recorded using photodissociation action spectroscopy, in which resonant absorption is registered by ejection of one or more NH_3 molecules following electronic excitation.⁸ Nothing is known about the mechanism of this fragmentation process, including whether it

occurs by fast, direct dissociation or by a relatively slow, statistical decay process. A detailed exploration of the photodissociation dynamics has the potential to provide important additional information, including a measurement of the Li–N bond dissociation energy. Consequently, in this work we report a velocity map imaging (VMI)⁹ study of the dissociation of electronically excited $\text{Li}(\text{NH}_3)_4$.

The VMI apparatus employed in this study has been described elsewhere.^{10,11} $\text{Li}(\text{NH}_3)_4$ is generated by laser ablation (*ca.* 10 mJ /pulse; 532 nm) of a solid lithium target in the presence of a mixture of NH_3 in helium (1:4 dilution). The gas mixture is held at a stagnation pressure of 7 bar prior to injection into the ablation zone. After flowing through a short clustering channel at room temperature, the $\text{Li}/\text{NH}_3/\text{He}$ mixture expands into vacuum and is then skimmed to form a molecular beam.

Photodissociation of $\text{Li}(\text{NH}_3)_4$ occurs between the repeller and extractor electrodes of the VMI-time-of-flight apparatus. The tunable near-infrared radiation was provided by an optical parametric oscillator (OPO; Continuum Panther) operating with pulse energies of ~ 500 $\mu\text{J}/\text{pulse}$ across the spectral range investigated ($5500 - 7000$ cm^{-1}). Parent molecules and fragments, $\text{Li}(\text{NH}_3)_3$ and $\text{Li}(\text{NH}_3)_2$, are then photoionized using a frequency doubled pulsed dye laser, at 282 nm.⁵ The resulting ions are then accelerated into the flight tube and are detected mass-selectively by a time-gated microchannel plate (MCP)/phosphor screen assembly coupled to a CCD camera. Images of the incident ions are then analyzed using a Polar Onion Peeling (POP) analysis program.¹²

The near-infrared spectrum of $\text{Li}(\text{NH}_3)_4$ is shown in Figure 1A. The spectrum is recorded in depletion mode, with $\text{Li}(\text{NH}_3)_4$ absorption registering as a negative-going $\text{Li}(\text{NH}_3)_4^+$ signal as a function of OPO wavenumber. The region shown in this spectrum spans the onset of the $\tilde{A}^2T_2 \leftarrow \tilde{X}^2A_1$ transition reported previously.⁸ Clear vibrational structure is evident in the lower frequency part of the spectrum ($6000\text{--}6500$ cm^{-1}) while at higher frequencies the spectrum assumes a quasi-continuous form. Figure 1B shows the corresponding signals recorded in the $\text{Li}(\text{NH}_3)^+$ and $\text{Li}(\text{NH}_3)_2^+$ fragment mass channels. At the lowest excitation energies $\text{Li}(\text{NH}_3)_3$ is the dominant photo-fragment, but $\text{Li}(\text{NH}_3)_2$ becomes increasingly important at higher energies until, beyond 6500 cm^{-1} , it is the dominant product.

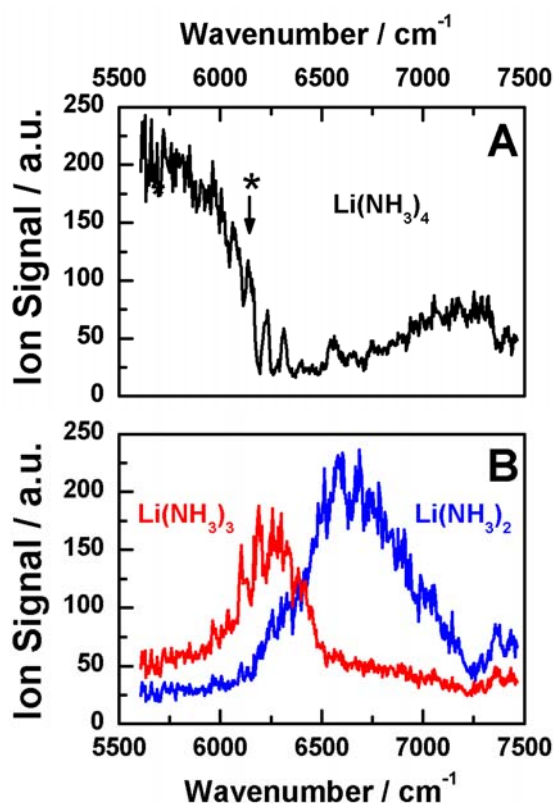


Figure 1. Near-infrared spectra recorded in (A) the Li(NH₃)₄ and (B) Li(NH₃)₃ [red] and Li(NH₃)₂ [blue] channels as a function of excitation wavenumber. See text for further details. The asterisk marks the excitation wavelength used for the velocity map image shown in Figure 2.

Figures 2A and 2B show the velocity map images of Li(NH₃)₃ with and without electronic excitation of Li(NH₃)₄ at 6145 cm⁻¹. This wavenumber corresponds to an intense feature in the Li(NH₃)₃ enhancement spectrum before the onset of the Li(NH₃)₂ product channel (see Figure 1B). The photofragmentation image (Figure 2B) is characterized by an intense central spot and a dominant broad, structureless feature extending to higher kinetic energy release (see Figure 2C). The central spot, which is also observed when the IR is blocked (see Figure 2A), is attributed to background Li(NH₃)₃ present in the molecular beam and can be subtracted as a background signal. The broad, higher kinetic energy signal arises from Li(NH₃)₃ photofragments following photodissociation of Li(NH₃)₄. As can be seen in Figure 2B, the Li(NH₃)₃ photofragment distribution is isotropic. Images have been recorded at several other IR wavenumbers extending up to 6900 cm⁻¹ and all show a profile analogous to that in Figure 2B.

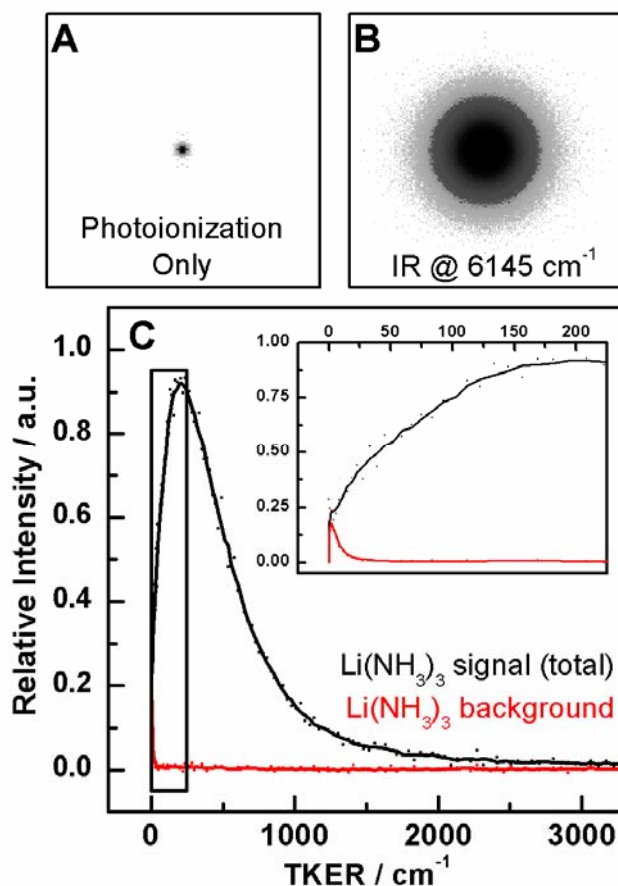


Figure 2. Velocity map images of $\text{Li}(\text{NH}_3)_3$. Panel A shows the background $\text{Li}(\text{NH}_3)_3$ in the molecular beam while panel B shows the image of the results of $\text{Li}(\text{NH}_3)_4$ photodissociation at 6145 cm^{-1} . Panel C gives the total kinetic energy release (TKER) spectrum extracted from the images shown in panels A and B. The most probable TKER is approximately 200 cm^{-1} , while the average TKER is approximately 410 cm^{-1} . The insert in panel C shows an expanded view of the low TKER profile.

Velocity map images were also recorded for the NH_3 fragments formed in the dissociation process. These fragments were ionized *via* a (2+1) REMPI scheme in the $70,050 - 70,550\text{ cm}^{-1}$ region.¹³⁻¹⁵ As a result of the large background signal arising from free NH_3 present in the molecular beam these images were of poorer quality than those observed gating the $\text{Li}(\text{NH}_3)_3$ product. Nevertheless, the TKER distributions were similar in both cases, peaking strongly at low (but non-zero) kinetic energies with an isotropic angular distribution.

The total kinetic energy release (TKER) spectra extracted from $\text{Li}(\text{NH}_3)_3$ photofragment images are shown in Figure 2C. The best *ab initio* estimates of the Li–N bond dissociation energy of $\text{Li}(\text{NH}_3)_4$ yield a value in the region of 3400 cm^{-1} .^{7,16} Given that $\text{Li}(\text{NH}_3)_4$ was excited at 6145 cm^{-1} for the TKER

spectrum in Figure 2C, and assuming that the $\text{Li}(\text{NH}_3)_4$ is initially cold, this leaves up 2745 cm^{-1} to be partitioned between kinetic energy release and internal excitation of the fragments. The mean TKER observed in the present work is *ca.* 410 cm^{-1} , with the most probable value *ca.* 200 cm^{-1} . These values indicate a strong preference for the production of highly internally excited photoproducts which, together with the lack of any apparent structure in the TKER spectrum, is characteristic of a statistical decay process.¹⁷

We have attempted to interpret the TKER distribution by modeling the product density of states. The highest possible internal energies will yield the highest density of internal states and thus, in a purely statistical decay process, the most likely products will be those with high internal excitation. Our simple model has focused only on the vibrational density of states (vDoS), derived from MP2 calculations of the harmonic vibrational frequencies of $\text{Li}(\text{NH}_3)_3$ coupled with the known fundamental vibrational frequencies of the co-product, NH_3 .⁷ To calculate the vDoS, we applied the Beyer-Swinehart algorithm^{17,18} for numerous available energy limits (*viz.* dissociation energies) and compared the calculated curves with the experimental TKER spectrum. Several such vDoS curves are shown in Figure 3. For $\text{TKER} > 300\text{ cm}^{-1}$ the rapid decline in signal intensity closely matches the decline in vDoS, supporting the idea of a statistical dissociation. Presumably, rapid internal conversion from the \tilde{A}^2T_2 to the \tilde{X}^2A_1 ground state occurs, followed by relatively slow statistical decay of the internally excited \tilde{X}^2A_1 state. The best agreement between the vDoS profiles and the experimental TKER spectra was obtained for a $\text{Li}(\text{NH}_3)_4$ dissociation energy of $D_0 = 3750 \pm 150\text{ cm}^{-1}$. This value represents an upper limit as our density of states calculations did not account for anharmonicity.

One important feature of the dissociation which is not captured by the idea of a purely statistical decay process is the presence of a maximum in the TKER profile, with zero production of very low TKER fragments. This is consistent with an energy barrier in the exit channel, which impedes the production of $\text{Li}(\text{NH}_3)_3$ with very low kinetic energies.¹⁹⁻²¹ Taking the ratio of the observed TKER profile with the predicted vDoS profile, it is possible to extract the experimental form of the

transmission probability across such a barrier as a function of TKER. The transmission probability curve in the region of the exit channel barrier is shown in Figure 3.

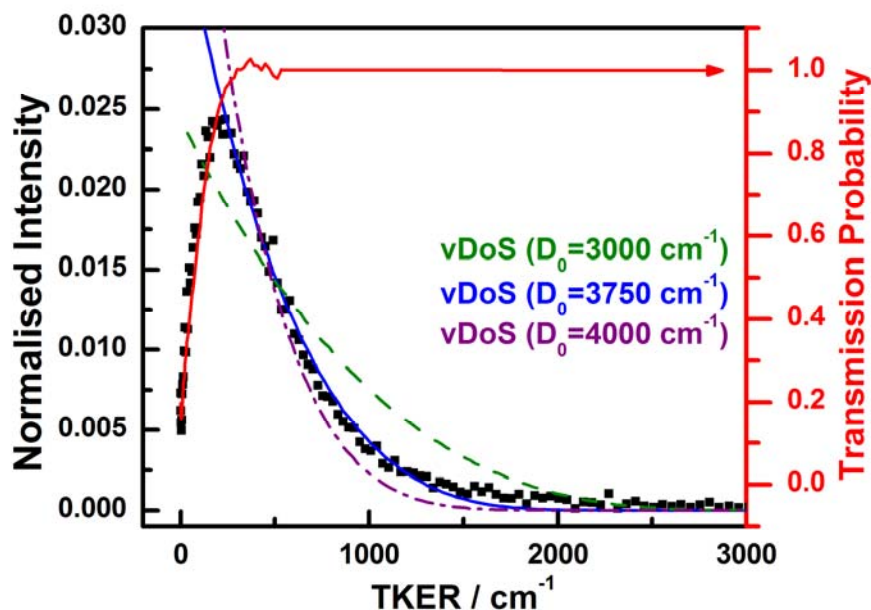


Figure 3. The experimentally observed $\text{Li}(\text{NH}_3)_3$ TKER distribution (filled points) overlaid with the vDoS calculated at $D_0 = 3000 \text{ cm}^{-1}$ (green), $D_0 = 3750 \text{ cm}^{-1}$ (blue), and $D_0 = 4000 \text{ cm}^{-1}$ (purple). The red curve is the experimental transmission probability calculated by dividing the experimental TKER by the best fitting ($D_0 = 3750 \text{ cm}^{-1}$) vDoS curve.

To gain insight into the barrier to $\text{Li}(\text{NH}_3)_4$ dissociation, the low TKER data has been modeled using a simple exit-channel Eckart potential barrier.^{22,23} The best fit to the experimental data indicates a barrier to dissociation for $\text{Li}(\text{NH}_3)_4$ of approximately $150 \pm 50 \text{ cm}^{-1}$. The origins of such a barrier are not fully understood but may be accounted for by an angular momentum barrier in the exit channel arising from the comparatively high angular momentum states of $\text{Li}(\text{NH}_3)_4$ which are populated in the molecular beam. The best estimate of the beam temperature is the rotational temperature of the NH_3 component, which has been determined via its $\tilde{C} - \tilde{X}$ REMPI spectrum to be $100 \pm 10 \text{ K}$. This represents a lower limit on the temperature of $\text{Li}(\text{NH}_3)_4$, which is likely to have residual internal energy due to the ablation and clustering process. The small rotational constant of $\text{Li}(\text{NH}_3)_4$ ($B = 0.08 \text{ cm}^{-1}$ from *ab initio* calculations), however, means that even at 100 K the expectation value of the total angular momentum quantum number, $\langle J \rangle$, is 24.5. This would introduce a centrifugal barrier of some 50 cm^{-1} . At a

rotational temperature of 300 K these numbers become 43.5 and 150 cm^{-1} , respectively, sufficient to account for the observations here.

In addition to $\text{Li}(\text{NH}_3)_3$ production, we have also investigated velocity map images for the $\text{Li}(\text{NH}_3)_2$ fragments, which result at higher excitation energies (see Figure 1). Two mechanisms could plausibly account for $\text{Li}(\text{NH}_3)_2$ production: (i) consecutive loss of two NH_3 molecules following $\text{Li}(\text{NH}_3)_4$ excitation or (ii) photodissociation of the primary $\text{Li}(\text{NH}_3)_3$ photofragment. Route (i) is unlikely given the theoretical estimate of the combined Li–N dissociation energies at $> 7800 \text{ cm}^{-1}$ (the Li–N dissociation energy of $\text{Li}(\text{NH}_3)_3$ is predicted to be substantially larger than $\text{Li}(\text{NH}_3)_4$) and the observation of $\text{Li}(\text{NH}_3)_2$ beginning at 6300 cm^{-1} . In principle, $\text{Li}(\text{NH}_3)_2$ could be generated by dissociation of hot $\text{Li}(\text{NH}_3)_4$ clusters but then one would expect a gradual rise in $\text{Li}(\text{NH}_3)_2$ signal as the excitation energy is increased rather than the relatively sharp onset observed. Multiphoton excitation by $\text{Li}(\text{NH}_3)_4$ also seems unlikely as experiments at different OPO intensities show little variation in the relative production of $\text{Li}(\text{NH}_3)_3$ and $\text{Li}(\text{NH}_3)_2$.

The TKER profile extracted from images recorded by gating the $\text{Li}(\text{NH}_3)_2^+$ signal is shown in Figure 4. Similar to $\text{Li}(\text{NH}_3)_3$ production, a maximum is also observed in the TKER distribution for $\text{Li}(\text{NH}_3)_2$. However, the TKER distribution of the latter is broader and the maximum shifted markedly to higher kinetic energies. Close examination of the $\text{Li}(\text{NH}_3)_2$ TKER distribution shows non-zero probability extending at least as far as 3000 cm^{-1} . These observations are consistent with the production of $\text{Li}(\text{NH}_3)_2$ by photofragmentation of internally excited $\text{Li}(\text{NH}_3)_3$, and, as with $\text{Li}(\text{NH}_3)_4$, provide evidence of a barrier to this process.

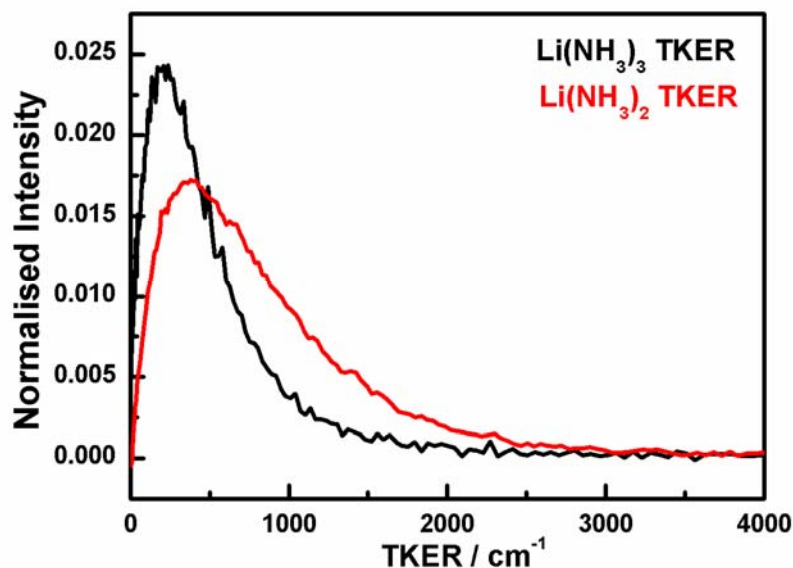


Figure 4. Comparison of the measured TKER for $\text{Li}(\text{NH}_3)_3$ production at 6145 cm^{-1} with that of $\text{Li}(\text{NH}_3)_2$ generated at 6505 cm^{-1} .

In summary this study is the first in which the total kinetic energy release from alkali-ammonia clusters has been investigated following photodissociation. Photolysis of $\text{Li}(\text{NH}_3)_4$ *via* its first excited electronic band system generates the primary photoproducts $\text{Li}(\text{NH}_3)_3 + \text{NH}_3$ and velocity map imaging shows that the products are formed internally hot, consistent with a statistical decay process. However, a maximum in the TKER profile implies a barrier in the exit channel preventing the generation of very low kinetic energy fragments. Modeling of the observed TKER profiles suggests a barrier height of *ca.* $150 \pm 50\text{ cm}^{-1}$ and a bond dissociation energy of $D_0 = 3750 \pm 150\text{ cm}^{-1}$ for $\text{Li}(\text{NH}_3)_4$ dissociation which, whilst representing an upper limit for the true value, is in good agreement with *ab initio* predictions. Finally, imaging of the $\text{Li}(\text{NH}_3)_2$ photofragments suggests that these originate from single-photon photodissociation of $\text{Li}(\text{NH}_3)_3$ clusters in the molecular beam, rather than thermal dissociation of hot $\text{Li}(\text{NH}_3)_3$ primary photoproducts.

Funding for this research was provided by the UK Engineering and Physical Sciences Research Council (grants EP/C012070 and EP/E062970). SRM is further grateful to the EPSRC for his Advanced Research Fellowship (2005-2010: EP/C01202X). WSH gratefully acknowledges funding from the Ramsay Memorial Fellowships Trust in the form of a Ramsay Memorial Fellowship.

REFERENCES

- (1) Boudaiffa, B.; Cloutier, P.; Hunting, D.; Huels, M. A.; Sanche, L. Low-energy electrons induced DNA strand breaks *M S-Medecine Sciences* **2000**, *16*, 1281-1283.
- (2) Thomas, J. M.; Edwards, P. P.; Kuznetsov, V. L. Sir Humphry Davy: Boundless chemist, physicist, poet and man of action *Chemphyschem* **2008**, *9*, 59-66.
- (3) Jacobson, L. D.; Herbert, J. M. Polarization-Bound Quasi-Continuum States Are Responsible for the "Blue Tail" in the Optical Absorption Spectrum of the Aqueous Electron *J. Am. Chem. Soc.* **2010**, *132*, 10000-10002.
- (4) Zurek, E.; Edwards, P. P.; Hoffmann, R. A Molecular Perspective on Lithium-Ammonia Solutions *Angew. Chem. Int. Ed.* **2009**, *48*, 8198-8232.
- (5) Salter, T. E.; Ellis, A. M. Structures of small Li(NH₃)(n) and Li(NH₃)(n)(+) clusters (n=1-5): Evidence from combined photoionization efficiency measurements and ab initio calculations *J. Phys. Chem. A* **2007**, *111*, 4922-4926.
- (6) Salter, T. E.; Mikhailov, V.; Ellis, A. M. Infrared photodissociation spectroscopy of Na(NH₃)(n) clusters: Probing the solvent coordination *J. Phys. Chem. A* **2007**, *111*, 8344-8351.
- (7) Salter, T. E.; Mikhailov, V. A.; Evans, C. J.; Ellis, A. M. Infrared spectroscopy of Li(NH₃)(n) clusters for n=4-7 *J. Chem. Phys.* **2006**, *125*, 034302.
- (8) Varriale, L.; Tonge, N. M.; Bhalla, N.; Ellis, A. M. Communications: The electronic spectrum of Li(NH₃)(4) *J. Chem. Phys.* **2010**, *132*, 161101.
- (9) Eppink, A.; Parker, D. H. Velocity map imaging of ions and electrons using electrostatic lenses: Application in photoelectron and photofragment ion imaging of molecular oxygen *Rev. Sci. Instrum.* **1997**, *68*, 3477-3484.
- (10) Hopkins, W. S.; Hamilton, S. M.; McNaughton, P. D.; Mackenzie, S. R. VUV photodissociation dynamics of diatomic gold, Au-2: A velocity map imaging study at 157 nm *Chem. Phys. Lett.* **2009**, *483*, 10-15.
- (11) Hopkins, W. S.; Woodham, A. P.; Plowright, R. J.; Wright, T. G.; Mackenzie, S. R. A velocity map imaging study of gold-rare gas complexes: Au-Ar, Au-Kr, and Au-Xe *J. Chem. Phys.*, *132*, 9.
- (12) Roberts, G. M.; Nixon, J. L.; Lecointre, J.; Wrede, E.; Verlet, J. R. R. Toward real-time charged-particle image reconstruction using polar onion-peeling *Rev. Sci. Instrum.* **2009**, *80*, 7.
- (13) Ashfold, M. N. R.; Dixon, R. N.; Little, N.; Stickland, R. J.; Western, C. M. The B ¹E" state of ammonia - sub-Doppler spectroscopy at vacuum ultraviolet energies *J. Chem. Phys.* **1988**, *89*, 1754-1761.
- (14) Ashfold, M. N. R.; Dixon, R. N.; Stickland, R. J. Molecular predissociation dynamics revealed through multiphoton ionization spectroscopy 2. The C' state of NH₃ and ND₃ *Chem. Phys.* **1984**, *88*, 463-478.
- (15) Nieman, G. C.; Colson, S. D. Characterization of the C' state of ammonia observed by 3-photon, gas-phase spectroscopy *J. Chem. Phys.* **1979**, *71*, 571-577.
- (16) Mierzwicki, K.; Latajka, Z. Nonadditivity of interaction in Li(NH₃)(n) and Li(NH₃)(n)(+) (n=1-4) clusters *Chem. Phys.* **2001**, *265*, 301-311.
- (17) Baer, T.; Hase, W. L. *Unimolecular Reaction Dynamics*; Oxford University Press: New York, 1996.
- (18) Beyer, T.; Swinehart, D. F. Algorithm 448: number of multiply-restricted partitions *Commun. ACM* **1973**, *16*, 379.

- (19) Ashfold, M. N. R.; Dixon, R. N.; Kono, M.; Mordaunt, D. H.; Reed, C. L. Near ultraviolet photolysis of ammonia and methylamine studied by H Rydberg atom photofragment translational spectroscopy *Phil. Trans. Roy. Soc.* **1997**, 355, 1659-1674.
- (20) Feltham, E. J.; Qadiri, R. H.; Cottrill, E. E. H.; Cook, P. A.; Cole, J. P.; Balint-Kurti, G. G.; Ashfold, M. N. R. Ketene photodissociation in the wavelength range 193-215 nm: The H atom production channel *J. Chem. Phys.* **2003**, 119, 6017-6031.
- (21) Waschewsky, G. C. G.; Kitchen, D. C.; Browning, P. W.; Butler, L. J. Competing bond fission and molecular elimination channels in the photodissociation of CH₃NH₂ at 222nm *J. Phys. Chem.* **1995**, 99, 2635-2645.
- (22) Atkins, P.; Friedman, R. *Molecular Quantum Mechanics*, 4 ed.; Oxford University Press: Oxford, 2005.
- (23) Eckart, C. The Penetration of a Potential Barrier by Electrons *Phys. Rev.* **1930**, 35, 1303.